Molecular Crystals and Liquid Crystals

Publication details, including instructions for authors and subscription information:
http://www.tandfonline.com/loi/gmcl20

Theoretical Performance Analysis of an Integrated Optic Filter Made of Glass Waveguides and POLICRYPS Holographic Gratings

Domenico Donisi [a], Antonio d'Alessandro [a], Rita Asquini [a] & Romeo Beccherelli [b]

[a] Department of Electronic Engineering, University of Rome "La Sapienza", via Eudossiana, Rome, Italy

[b] CNR-Institute for Microelectronics and Microsystems

Version of record first published: 22 Sep 2010

To cite this article: Domenico Donisi, Antonio d'Alessandro, Rita Asquini & Romeo Beccherelli (2007): Theoretical Performance Analysis of an Integrated Optic Filter Made of Glass Waveguides and POLICRYPS Holographic Gratings, Molecular Crystals and Liquid Crystals, 465:1, 227-237

To link to this article: http://dx.doi.org/10.1080/15421400701206022

Mol. Cryst. Liq. Cryst., Vol. 465, pp. 227–237, 2007

ISSN: 1542-1406 print/1563-5287 online
DOI: 10.1080/15421400701206022

Taylor & Francis
Taylor & Francis Group

Theoretical Performance Analysis of an Integrated Optic Filter Made of Glass Waveguides and POLICRYPS Holographic Gratings

Domenico Donisi
Antonio d'Alessandro
Rita Asquini
Department of Electronic Engineering, University of Rome "La Sapienza", via Eudossiana, Rome, Italy

Romeo Beccherelli
CNR-Institute for Microelectronics and Microsystems

We present the theoretical study and the simulation of the optical field propagation in a guided wave tuneable optical filter using a composite material grating. A numerical analysis of the optical propagation has been performed by using a 3D semivectorial BPM (Beam Propagation Method) based software and the results have been compared with a matrix-transfer approach based on the effective index method. The dependency of the filter response on the index modulation depth (Δn), the length and the thickness of the grating have been also analyzed. Performance of chirped and apodized gratings were also studied. The optical filter reflection and transmission spectral responses in terms of full width at half maximum (FWHM) have been calculated.

Keywords: composite materials; holographic Bragg gratings; integrated optical filter

INTRODUCTION

Optical tuneable filters are essential components in Fiber-To-The-Home wavelength division multiplexing optical communication systems and in optical sensor systems.

Various tuneable/active filters have been demonstrated, based on acousto-optical [1], thermo-optical [2] or electro-optical [3] effect.

Address correspondence to Domenico Donisi, Department of Electronic Engineering, University of Rome "La Sapienza", via Eudossiana, 18, Rome 00184, Italy. E-mail: domenico.donisi@uniroma1.it

However all these technologies have limitations, either in terms of insertion loss, power consumption, scalability or integration.

In this article we will study a novel integrated tuneable filter using a holographic Bragg grating, which introduces advantages in terms of compactness, manufacturing requirements, high performance and low power consumption with respect to the state of the art. The device based on composite material gratings continues to stimulate an extensive research activity to realize permanent and electrically switchable diffraction gratings that can be used for optical communications, optical data storage and processing.

STRUCTURE OF THE DEVICE

A picture of a fabricated prototype of the optical filter is shown in Figure 1. The circular opaque area, with a diameter of 1 cm, corresponds to the grating whose period is about 2.5 μm. The device is made of double ion-exchanged glass single mode optical channel waveguide and a POLICRYPS (POlymer LIquid CRYstal Polymer Slices) [4] grating as a cladding layer. We use a reliable and reproducible K^+–Na^+/Ag^+–Na^+ double ion-exchanged process in BK7 glass to obtain low losses (<1 dB/cm) and high index-contrast ($\Delta n_{wg} \sim 0.04$) optical waveguides [5]. The refractive index profile of the waveguide

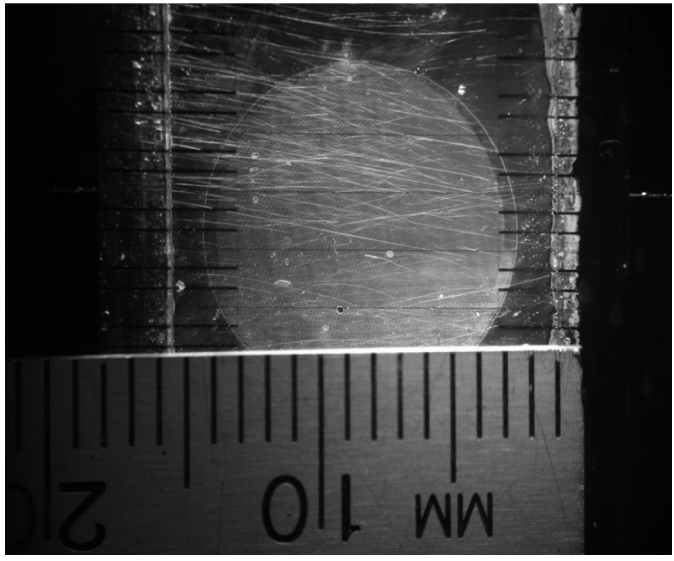

FIGURE 1 Snapshot of the prototype of an IO filter using POLICRYPS.

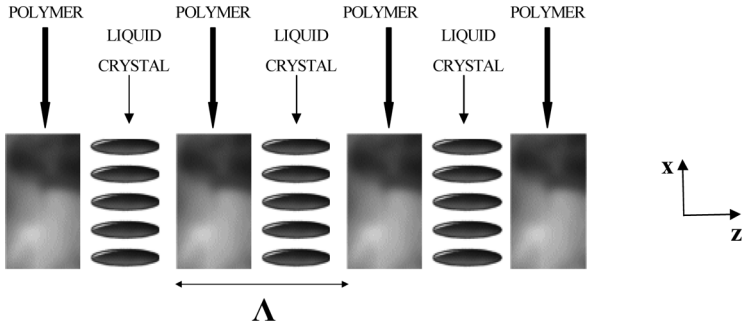

FIGURE 2 Sketch of the POLICRYPS grating structure.

depends on the process parameters, especially molar concentration of KNO_3 and $AgNO_3$, and process duration. A typical POLICRYPS grating consists of polymer slices alternated with films of regularly aligned nematic liquid crystal (NLC), which can be switched by applying an adequate electric field with a proper electrodes configuration. The polymer used in POLICRYPS grating is NOA 61, whose refractive index at $\lambda = 1550\,\text{nm}$ is $n_P = 1.5419$, and the liquid crystal is E7, whose ordinary and extraordinary refractive indices are respectively $n_o = 1.5$ and $n_e = 1.689$ at 20°C [6,7]. The boundary conditions imposed by the confining walls of the polymers in the POLICRYPS ensures that the LC alignment is along the z-axis as sketched in Figure 2, showing schematically the top view of the grating structure. The pitch of the POLICRYPS grating depends on the holographic interference angle used in the grating writing process and can typically be tuned between 0.2 and 11 μm.

Since in most of applications a single mode propagation is required to avoid multipath dispersion of the light signals, the transversal dimensions of the waveguided device are designed to allow propagation only of the fundamental mode in the working optical band. The POLICRYPS filter structure includes aluminum coplanar electrodes, for an in-plane reorientation of the NLC molecules between the polymer slices, by exploiting the electro-optic properties of the POLICRYPS grating [8]. The gap between the electrodes, where the waveguides are located, is wide enough to avoid optical losses induced by influence of aluminum on the light propagation in the optical channels.

PRINCIPLE OF WORKING

The electro-optical effect plays a fundamental role in the device operation. Therefore in the following it is explained how a control electric

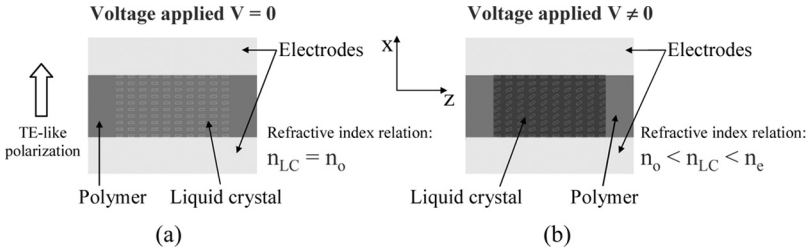

FIGURE 3 Top view of the device and sketch of the working principle. (a) Without applied voltage and (b) with applied voltage.

field acts on the filter behaviour. Figure 3 shows the top view and the working principle of the device. In the absence of external electric field, the director of the LC molecules is aligned normally to the polymer/LC interface as it is shown in Figure 3a. The desired tilt of the NLC molecules and the corresponding required profile of the refractive index is obtained by applying a suitable control voltage. Such LC reorientation makes only guided light with TE-like polarization to "see" a refractive index modulation of the overlaying hybrid cladding which acts as the optic field perturbation element. In particular a TE-like optical field propagating along (Oz) will see the ordinary index n_o of the LC when no external signal is applied. Applying an external electrical field (see Figure 3b), the molecules rotate in the plane (xz) and the TE-like optical field will see a higher refractive index n of the LC (between n_o and n_e). The tuning capability of the filter depends on the possibility to change the effective refractive index (n_{eff}) of the guided mode by controlling the mismatch between LC and polymer refractive indices ($\Delta n = n_P$-n_{LC}). To understand the operation of the device and how the spectral response is correlated with the modal and geometrical properties of the filter in terms of bandwidth and shape, it is useful to consider as the starting point the situation of complete matching of LC and polymer refractive indices corresponding to an absence of the grating. By changing the voltage value a mismatch Δn is induced and the Bragg grating appears. The index mismatch influences n_{eff} and so the Bragg wavelength λ_B is tuned according to the formula:

$$m\lambda_B = 2n_{eff}\Lambda \tag{1}$$

where m is the diffraction order and Λ is the grating period.

The reflectivity (the transmissivity) increases (decreases) as Δn increases for a fixed grating length, defined as the product between the number of grating planes (M) and the pitch of the grating (Λ). Similarly, as the length of the grating increases, so does the resultant

reflectivity (for a fixed Δn). The full width at half-maximum (FWHM) bandwidth of a uniform Bragg grating is strongly dependent on the grating length, Δn and the order of the grating period. A general expression for the approximate full width at half-maximum bandwidth of a grating is given by:

$$\Delta\lambda = \lambda_B \alpha \sqrt{\left(\frac{\Delta n}{2n_{av}}\right)^2 + \left(\frac{1}{2M}\right)}$$

where M is the number of the grating periods and n_{av} is the average refractive index of a uniform Bragg grating. The parameter α is about 1 for strong gratings (for grating with near 100% reflection) whereas $\alpha \sim 0.5$ for weak gratings [9]. Typically the grating period required for first-order reflection at 1550 nm is approximately 0.5 μm. In order to obtain small bandwidths it is possible to work with Bragg gratings that reflect light in the third or fifth order, which have a grating pitch of approximately 1.5 and 2.5 μm, respectively.

SIMULATION RESULTS

A matrix-transfer approach based on the effective index method has been used to describe the behaviour of the grating in cases of almost

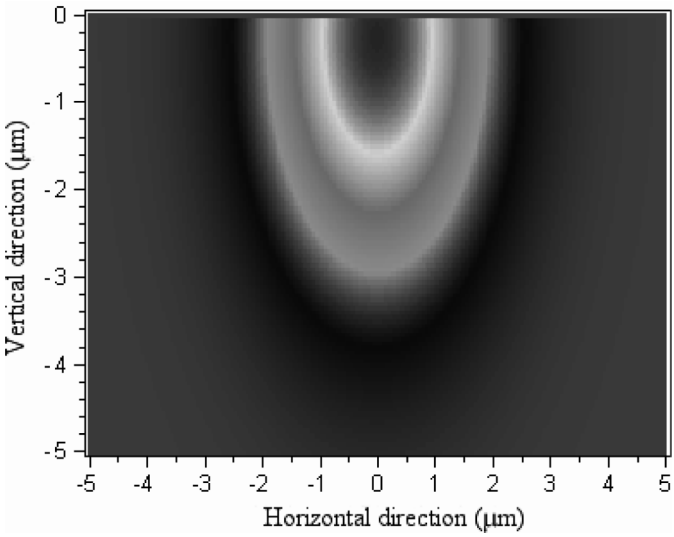

FIGURE 4 Refractive index gaussian-profile of the optical channel waveguide.

periodic grating. In our case, the waveguide is weakly coupled to a uniform grating and we have observed that 3D numerical analysis based on the coupled-mode theory shows a good agreement with effective index method [10]. Therefore in the following we will use the software *GratingMOD* based on the coupled-mode theory and provided by *RSoft*. *GratingMOD* is an integrated software package capable of analyzing complex grating structures.

In the first set of simulations it has been assumed to have a uniform change of the LC index of refraction over the grating length and a proper pitch of the grating. We have considered a K^+-Na^+/Ag^+-Na^+ gaussian shaped buried waveguide (with a mask opening width of 6 μm) diffused into a BK7 glass substrate having refractive index

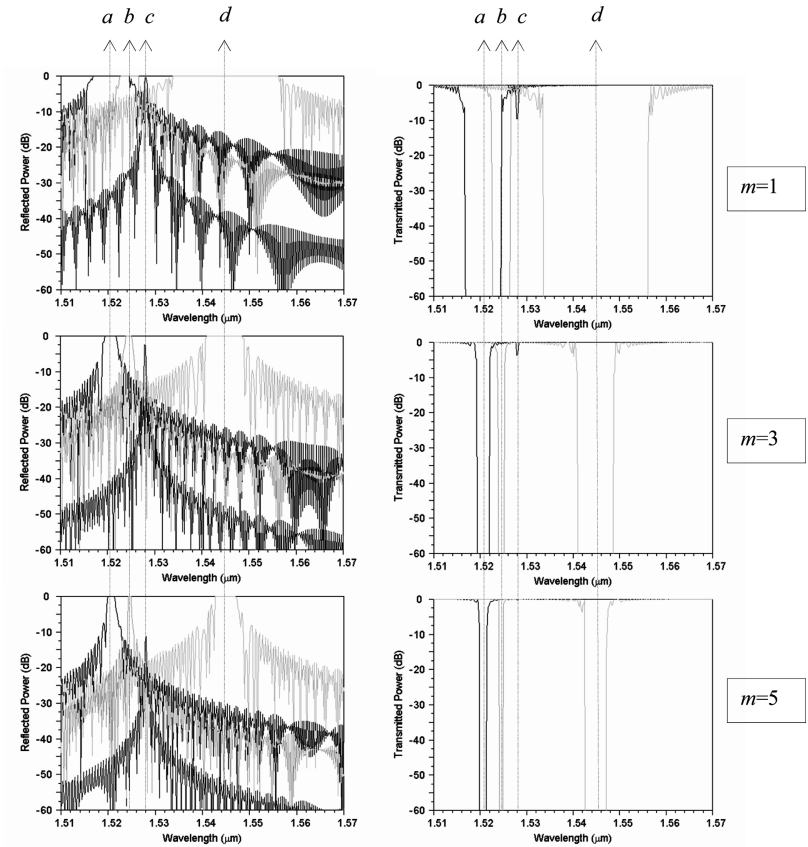

FIGURE 5 Optical filter reflection and transmission spectral response.

TABLE 1 Device Performance for Different Grating Step-Index Modulations (Δn) and Diffraction Orders

$\Lambda = 0.5\,\mu\text{m}(m=1)$	$\Delta n(n_{POL} - n_{LC})$	FWHM (nm)
a	0.0419	9.08
b	0.01	4.43
c	0.001	0.69
d	− 0.0419	23.14
$\Lambda = 1.5\,\mu\text{m}(m=3)$	$\Delta n(n_{POL} - n_{LC})$	FWHM (nm)
a	0.0419	3.18
b	0.01	1.72
c	0.001	0.41
d	− 0.0419	8.38
$\Lambda = 2.5\,\mu\text{m}(m=5)$	$\Delta n(n_{POL} - n_{LC})$	FWHM (nm)
a	0.0419	1.88
b	0.01	0.84
c	0.001	0.39
d	− 0.0419	4.89

distribution in the transversal plane *xy* given by [11]:

$$\begin{aligned} n(x,y) &= n_{sub} + \Delta n_{sub}\left\{\exp\left[-\frac{x}{h_{diffx}}\right]^2 \exp\left[-\frac{(y+d_{bur})}{h_{diffy}}\right]^2\right\} \\ \forall y > 0 &\Rightarrow n(x,y) = 1 \quad (air) \\ \forall |x| > \frac{w}{2} &\Rightarrow n(x,y) = n_{sub} \\ \forall y < -h &\Rightarrow n(x,y) = n_{sub} \end{aligned} \tag{3}$$

where n_{sub} and Δn_{sub} are the substrate and the waveguide gap refractive indices respectively, w and h are the width and height of the channel

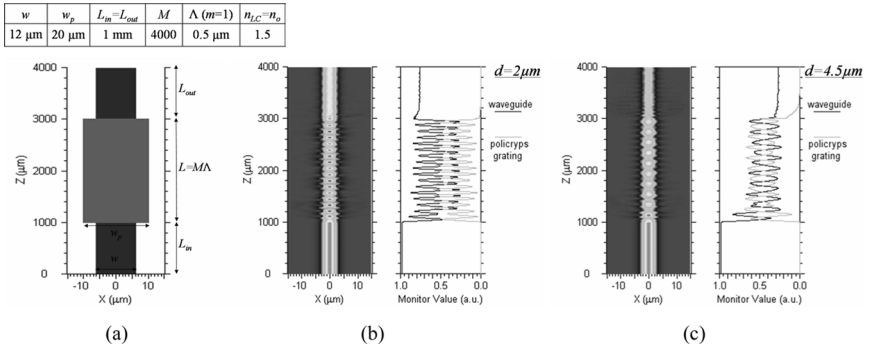

FIGURE 6 Power monitor for different cell thickness.

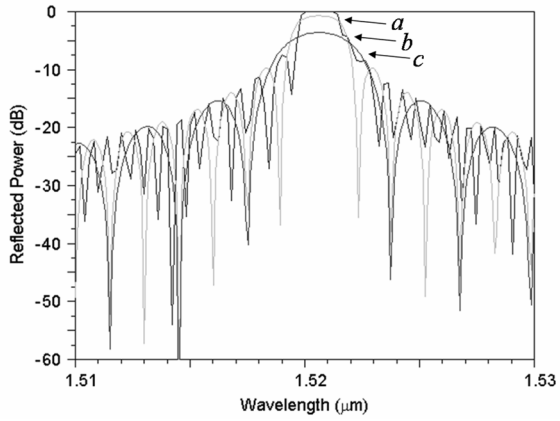

m=5; n_{LC}=n_o	M
a	4000
b	200
c	100

FIGURE 7 Filter response dependence on the grating length.

waveguide, h_{diffx} and h_{diffy} are the transversal diffusion lengths and d_{bur} is the burying depth.

The values assumed in the simulation for a typically fabricated waveguide by using double ion-exchange process are: $w = h = 12\,\mu m$, $h_{diffx} = 2\,\mu m$, $h_{diffy} = 2.8\,\mu m$, $d_{bur} = 0.25$, $\Delta n_{sub} = 0.04$. The transversal refractive index profile of the optical channel waveguide used in the simulations is sketched on Figure 4.

The optical filter reflection and transmission spectral response has been calculated in order to demonstrate the strong dependence of FWHM on the order of the grating period and the mismatch Δn. Figure 5 shows calculated reflection and transmission spectra for a fixed grating length ($M = 4000$) and a cell thickness of $2\,\mu m$, by varying Δn from 0.0419 to -0.0419 and selecting four particular values. In particular three different grating periods, corresponding to the first, third and fifth order are respectively carried out. In Table 1 the performance of the device for different grating step-index modulations (Δn) are reported. In particular Table 1 indicates that it is necessary to operate with higher diffraction orders to work with small bandwidths. Furthermore the filter bandwidth decreases as the Δn decreases according to an external applied voltage.

The influence of the grating thickness on the filter performance has been evaluated in terms of loss. Figure 6 shows the schematic top view of the device (6a) and the output power for two different cell thicknesses: $2\,\mu m$ (6b) and $4.5\,\mu m$ (6c). It is evident how the losses increase as the grating thickness increases because of a stronger perturbation.

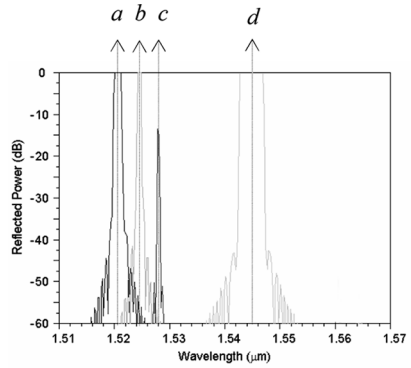

(a)

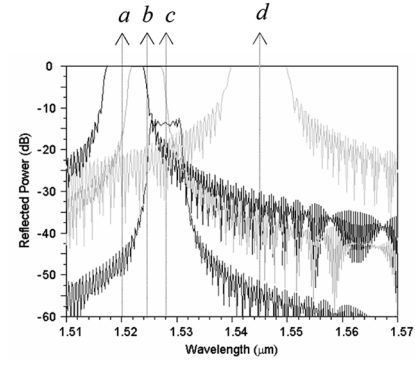

(b)

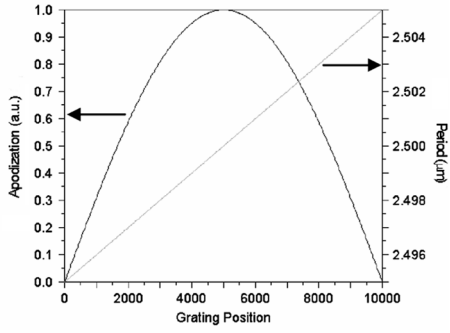

(c)

FIGURE 8 (a) Reflection spectral response of an apodized grating. (b) Reflection spectral response of a chirped grating. (c) Apodization profile and period variation along the grating position.

TABLE 2 Device Performance for an Apodized (a) and a Chirped (b) Grating

$\Lambda = 2.5\,\mu m (m = 5)$	$\Delta n(n_{POL} - n_{LC})$	FWHM (nm)
a	0.0419	1.43
b	0.01	0.8
c	0.001	0.38
d	− 0.0419	4.42
$\Lambda = 2.5\mu m (m = 5)$	$\Delta n(n_{POL} - n_{LC})$	FWHM (nm)
a	0.0419	7.42
b	0.01	6.42
c	0.001	5.76
d	− 0.0419	11.07

To show the filter response dependence on the grating length, we have varied the number of the grating periods as well as the total length. In Figure 7 it is possible to see how the reflectivity increases as the length of the grating increases in the case of $\Delta n = 0.0419$ and for the fifth order of the grating period ($m = 5$). So far we have analyzed the performance of the optical filters by considering a non-chirped and non-apodized grating. This certainly introduces side lobes in the spectral response, which are due to multiple reflections to and from opposite ends of the grating region. There are two different techniques to attenuate these side lobes: the grating apodization and chirping. The first one consists of a function assisted Δn modulation along the axis of optical propagation, while the second one provides a variation of the grating pitch along the same direction. The obtained results with these two different methods are shown in Figure 8a and 8b. Moreover it is possible to observe the apodization profile and the period variation along the grating position in Figure 8c. The simulations have been performed by using a grating pitch of 2.5 μm. The optical filter reflection responses have been calculated by varying Δn from 0.0419 to -0.0419 and selecting the same four values used in the previous simulations. In Table 2 the performance of the device in terms of FWHM are reported.

CONCLUSIONS

We reported the performance analysis of a novel integrated tuneable filter using a polymer and liquid crystal holographic grating on glass waveguides. The most important device feature is the possibility to

induce a grating refraction index modulation by exploiting the electro-optical effect in the liquid crystal slices of the POLICRYPS. Using an approach based on the coupled-mode theory we have computed the optical filter reflection and transmission spectral response and characterized the filter performance in terms of bandwidth for different diffraction orders. It has been calculated a FWHM of about 0.4 nm by operating to the fifth grating diffraction order with a $\Delta n = 10^{-3}$. It has been shown that such filter can exhibit a broad tuning range with a small mismatch between the polymer and the LC refractive index. In particular it has been evaluated a tuning range of about 25 nm by changing the LC refractive index from n_o to 1.5838. It means that such filter is a good candidate as a high performance and low power consumption device.

REFERENCES

[1] Smith, D. A., d'Alessandro, A., Baran, J. E., Fritz, D. J., Jackel, J. L., & Chakrawarthy, R. S. (1996). Multiwavelength performance of an apodized acousto-optic switch, *J. Lightwave Technol.*, *14*(9), 2044–2051.

[2] Agrawal, G. P. (2004). *Lightwave Technology: Components and Devices*, 1st ed., John Wiley & Sons Inc. Hoboken, New Jersey.

[3] Heisemann, F., Buhl, L. L., & Alferness, R. C. (1987). Electro-optically tunable narrowband TI:$LiNbO_3$ Wavelength Filter, *Electron. Lett.*, *23*(11), 572–574.

[4] Caputo, R., De Sio, L., Veltri, A., & Umeton, C. (2004). Development of a new kind of switchable holographic grating made of liquid-crystal films separated by slices of polymeric material, *Opt. Lett.*, *29*(11), 1261–1263.

[5] Zou, J., Zhao, F., & Chen, R. T. (2002). Two-step K+-Na+ and Ag+−Na+ ion-exchanged glass waveguides for C- band applications, *Appl. Opt.*, *41*(36), 7620–7626.

[6] Warenghem, M., Lab. de Physico-chimie des Interfaces et Applications, Lens, FR, private communications, October 2000.

[7] Li, J., Wu, S. T., Brugioni, S., Meucci, R., & Faetti, S. (2005). Infrared refractive indices of liquid crystals, *J. Appl. Phys.*, *97*, 073501.

[8] d'Alessandro, A., Asquini, R., Gizzi, C., Caputo, R., Umeton, C., Veltri, A., & Sukhov, A. V. (2004). Electro-optic properties of switchable gratings made of polymer and nematic liquid crystals slices, *Opt. Lett.*, *29*(12), 1405–1407.

[9] Russel, P. St J., Archambault, J.-L., & Reekie, L. (1993). *Phys. World*, *41*.

[10] Winick, K. A. (1992). Effective-index method and coupled-mode theory for almost-periodic waveguide gratings: A comparison, *Appl. Opt.*, *31*(6), 757–764.

[11] Auger, P. L. & Najafi, S. I. (1994). Potassium- and silver-double-ion-exchanged slab glass waveguides: characterization and modeling, *Appl. Opt.*, *33*(16), 3333–3337.